Article

Journal of
Nanoscience and Nanotechnology
Vol. 17, 1796–1805, 2017
www.aspbs.com/jnn

Characteristics of Nanoscale Active Oxide in Enhancing Penetration Capability of Surfactant Flux Assisted TIG Welding

Kuang-Hung Tseng* and Chih-Sheng Chen

Institute of Materials Engineering, National Pingtung University of Science and Technology, Pingtung 91201, Taiwan

The penetration capability (PC) of different TiO_2 particle size assisted TIG welding of UNS S17400 stainless steel was investigated. Microscale TiO_2 (MST) and nanoscale TiO_2 (NST) powders mixed with pure water (100% W), pure acetone (100% A), or a water/acetone (W/A) solvent were used as the surfactant flux (SF). The role of a nanoscale active oxide in enhancing the PC of the SF assisted TIG (TIG-SF) welding of stainless steel is also demonstrated. The results show that NST powder requires a significantly greater amount of solvent to create a paste-like SF compared to MST powder. The 80% W/20% A ratio was the preferred solvent for mixing both the MST and NST powders. During NST flux assisted TIG welding of UNS S17400 stainless steel, an electrical insulation bond (EIB) was more easily formed and sufficient oxygen concentration (OC) was also more quickly obtained. Consequently, the use of NST ingredient could further enhance the PC of the TIG-SF welding of UNS S17400 stainless steel, as compared to the use of MST ingredient. This study proposes that the oxide used in the TIG-SF welding of stainless steels must have three key features: a high electrical resistance, low thermal stability, and small particle size.

Keywords: Microscale TiO_2, Nanoscale TiO_2, Penetration Capability, Surfactant Flux, TIG Welding.

1. INTRODUCTION

Precipitation hardening stainless steel (PHSS) is a Fe–Cr–Ni series stainless steel that contains other alloying elements such as Cu, Al, Ti, Nb, or Mo, allowing it to be strengthened or hardened by treatment with a solution, quenched, and then artificially aged. PHSS is generally categorized into three grades:[1] the martensitic grade (such as UNS S17400 stainless steel), the semi-austenitic grade (such as UNS S17700 stainless steel), and the austenitic grade (such as UNS S66286 stainless steel). PHSS, like martensitic stainless steels, can be significantly strengthened or hardened by heat treatment, but in most environments, it has a corrosion resistance comparable to austenitic stainless steel. Typical applications for PHSS include steam turbine blades, nuclear reactor parts, aircraft parts, flat springs, spring holders, pressure vessels, retaining rings, diaphragms, fasteners, shafts, chains, valves, and gears, among others. TIG welding of PHSS produces high-quality welds with a clean, smooth surface. However, TIG welding has shallower penetration and lower deposition, particularly for a single-pass procedure, as well as no groove preparation. Its ability to join thick sections of PHSS is thus restricted.

TIG-SF welding, in which ionic compounds are added into a molten pool (MP), is a modified TIG welding process developed by the E.O. Paton Electric Welding Institute (Ukraine).[2] Recently, increases in productivity due to TIG-SF welding have been observed in a wide range of industrial sectors, including aerospace, military, petrochemical, power generation, and shipbuilding. The SF is one of the key factors in increasing the depth of the TIG-SF welds.[2–7] The ingredient of the SF varies according to the physicochemical, mechanical, and metallurgical properties of metal to be welded. Active oxides are most commonly used for the TIG-SF welding of metals. In particular, TiO_2 is widely selected as an ingredient for SF. For example, a SF consisting of 6% TiO_2, 6% SiO_2, and 88% $Na_2Ti_3O_7$ has been reported for plain carbon steel;[8] a SF consisting of 35% SiO_2, 25% TiO_2,

*Author to whom correspondence should be addressed.

 1533-4880/2017/17/1796/010 doi:10.1166/jnn.2017.13004

14% Cr_2O_3, 12% MoO_3, 7% MoS_2, and 7% halide has been reported for austenitic stainless steel;[9] a SF consisting of 17.7% TiO, 20.4% TiO_2, 22.8% Ti_2O_3, 29.7% NiO, and 9.4% $Mn_{15}Si_{26}$ has been reported for nickel-based alloy;[10] a SF consisting of 58% Cr_2O_3, 28% TiO_2, and 14% La_2O_3 has been reported for aluminum alloy;[11] a SF consisting of 60% $ZnCl_2$, 15% Cr_2O_3, 15% TiO_2, and 10% SiO_2 has been reported for magnesium alloy.[12]

A nanoscale particle is defined as a particle with a size in the range of 1–100 nm from zero to three dimensions,[13] which exhibits strong size-dependent physicochemical properties compared to a microscale particle of the same material,[14] due to the unique structure of the nanoscale particle. In the TIG-SF welding of metals, active oxide powders with particle sizes of 40–100 μm have mostly been used as the ingredient of a SF. Note that the particle size of the powder has a significant influence on particle–particle cohesive forces and particle-substrate adhesive forces. There is limited data available regarding the influence of nanoscale active oxides on the depth of the TIG-SF welds compared to microscale active oxides. In this study, TiO_2 was selected as the SF ingredient to investigate the influence of its particle sizes on the shape and size of TIG-SF welds. The impact of various SF densities on the depth of the TIG welds made with the MST and NST ingredients was also investigated, and the results were compared. Furthermore, choosing a suitable solvent in which to mix the powder to achieve sufficient coatability of the SF is important. The relationship between the solvent and the ingredient was thus also discussed. It is expected that better understanding the characteristics of nanoscale active oxides in enhancing the PC of the TIG-SF welding will further develop new SF formulas for various metals.

2. EXPERIMENTAL DETAILS

Solution-annealed UNS S17400 stainless steel was used as the base metal. Table I presents the chemical composition of the base metal, with the major components determined using a GDS-750A glow discharge spectrometer. The UNS S17400 stainless steel is a martensitic grade PHSS that has high-strength, excellent corrosion resistance, and good weldability.[15] The steel was cut by a band-sawing machine into specimens with 160×150 mm dimensions, for an 8 mm thick plate. Prior to welding, the surface of the specimens was lightly ground using 320 grit SiC abrasive paper to remove all visible surface impurities, followed by washing with acetone and then drying with a clean cheesecloth.

Powdered TiO_2 of various particle size grades was ordered from the manufacturer and used in this study. The particle size distributions of TiO_2 powder were differentiated into two grades: 74 ± 4 μm MST ingredient with 99.6% purity; 18 ± 6 nm NST ingredient with 99.9% purity. The TiO_2 powder was mixed with a solvent to form a wet SF, and then coated onto the surface of the specimen to be welded. The solvent volatilized, leaving a layer of the dried SF on the specimen surface.

The specimen with the TiO_2 coating was rigidly clamped by a specially designed fixture. TIG welding with a straight polarity was performed using semi-automatic equipment, in which a welding torch was moved along the centerline of the specimen. The welding torch was perpendicular to the specimen surface. During welding, no filler metal was added to the MP. The welding speed was set at 130 mm per minute, and three levels of welding current (150 A, 200 A, 250 A) were investigated. The power supply used in this welding machine had a constant current mode, maintaining a stable operating current irrespective of fairly large voltage changes. Tungsten electrode had an AWS classification of EWLa-1.5 and a rod diameter of 3.2 mm. The electrode tip had an included grind angle of 60° and a flat surface with a smaller diameter. The distance between the electrode tip and the specimen surface was kept at 2.0 ± 0.1 mm. High-purity grade (99.996%) argon gas with a flow rate of 15 liters per minute was used to create a protection of inert atmosphere around the tungsten electrode, the electric arc, and the liquid metal.

Following welding, the samples were cut at a section perpendicular to the longitudinal axis of the welded joint. All samples were then mounted, ground, polished, and etched. The etching was carried out in an electrolyte solution containing 10 g of oxalic acid crystals in 100 ml of deionized water. The weld shape was photographed using a stereo microscope, and its size was measured using a toolmaker's microscope. Each listed value of the weld size is an average of three readings.

3. RESULTS AND DISCUSSION

3.1. X-ray Diffraction (XRD) Analysis of TiO_2 Powder

In this study, the crystal type of the TiO_2 powder was analyzed by XRD using a D8 ADVANCE X-ray diffractometer operating at 40 kV, 40 mA, and with CuKα radiation. The XRD data were collected within the scattering

Table I. Chemical composition of UNS S17400 stainless steel.

	Chemical element (in wt.%, balance Fe)								
Specification	C	Mn	Si	P	S	Cr	Ni	Cu	Nb + Ta
ASTM A564	0.07 max	1.00 max	1.00 max	0.040 max	0.030 max	15.0–17.5	3.0–5.0	3.0–5.0	0.15–0.45
GDS-750A	0.03	0.67	0.38	0.019	0.012	15.32	4.64	3.49	0.22

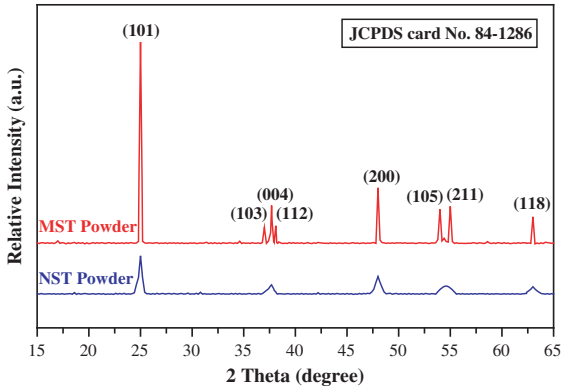

Figure 1. XRD pattern of TiO_2 powders used in this study.

angle range of 15–65°, with a step increment of 0.075° and a counting time of 4 s per step. The XRD patterns of both the MST and NST powders were then compared with reference to the Joint Committee on Powder Diffraction Standards database.

Figure 1 shows the XRD pattern of the TiO_2 powder used in this study. The results show that the XRD patterns of both the MST and NST powders exhibited strong diffraction peaks at 25°, 37–38°, 48°, 54–55°, and 63°. All the diffraction peaks are well matched with the standard spectrum (JCPDS card No. 84-1286). The observed diffraction peaks corresponding to the reflection planes (101), (103), (004), (112), (200), (105), (211), and (118) provide clear indicate that both the MST and NST powders are primarily in the anatase crystal. The XRD patterns also show that the diffraction peaks of the NST powder are much broader than those of the MST powder. The results provide evidence that the NST powder has a very small particle size compared to MST powder. In addition, the intensity of the diffraction peaks of the NST powder is much lower than that of the MST powder, suggesting that the NST powder is composed of irregular crystals.

3.2. Experimental Evaluation of TiO_2 Coating

Figure 2 shows the preparation process for obtaining the TiO_2 coating. The UNS S17400 stainless steel specimen was ground to produce a consistent surface finish. A constant weight of powder was mixed with the water or acetone in a beaker, followed by stirring with a glass rod to obtain a SF. The SF was then coated onto the ground surface of the specimen using a paintbrush. It is essential for the SF to be in a paste-like state with good coatability. It is thus necessary to choose an appropriate amount of solvent according to the powder characteristics. Figure 3 shows the SF states produced by adding different amounts of solvent to 250 mg of MST or NST powder. In this trial, the coated SF can be divided into three distinct states: the dough-like state (less solvent added; poor mixed state), the paste-like state (appropriate amount of solvent added;

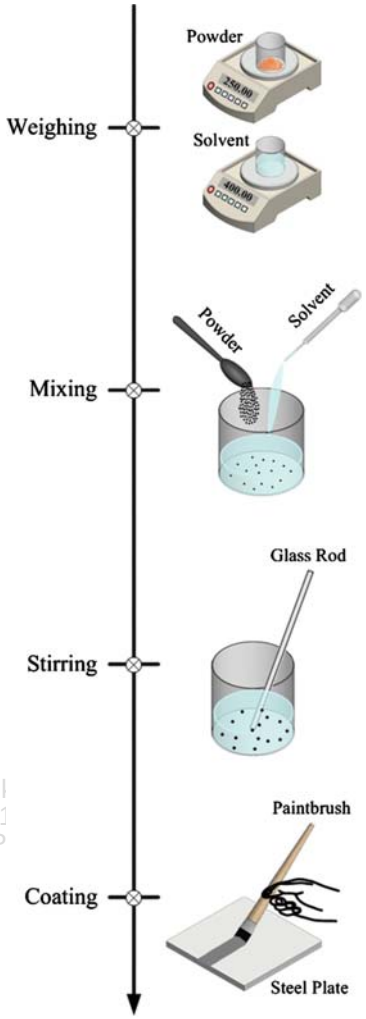

Figure 2. Preparation process for obtaining SF coating.

good mixed state), and the over-diluted state (more solvent added; poor mixed state). As presented in Figure 3, 250 mg of MST powder mixed with 0.3 to 0.6 ml of solvent and 250 mg of NST powder mixed with 2.5 to 3.4 ml of solvent both resulted in a paste-like SF. The results show that the NST powder requires a far greater amount of solvent to produce a SF with a paste-like state compared to the MST powder, due to a higher specific surface area of the smaller particles.

Several SF coating trials were performed to determine the best solvent for the MST and NST powders. Figure 4 shows the appearance of the TiO_2 coating obtained with the various solvents. In this trial, 250 mg of the MST and NST powders were mixed with 0.45 ml and 2.9 ml of the solvent, respectively, to create a paste-like SF. In other words, the mixing ratio by weight of the MST powder to the solvent was 1:1.6, while that of the NST powder to the solvent was 1:10.5. In addition, the coatability of

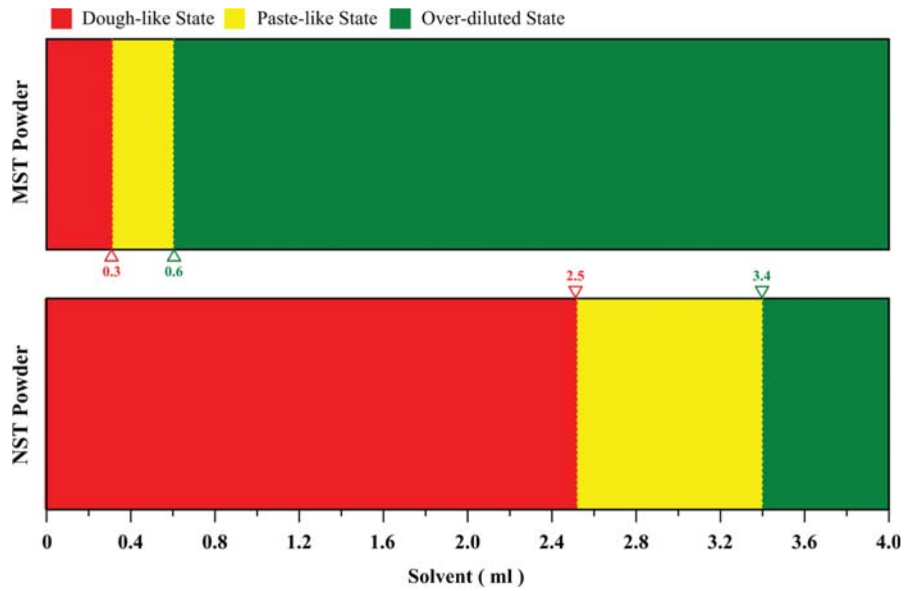

Figure 3. SF states produced by adding different amounts of solvent to 250 mg of MST or NST powder.

the SF was characterized by its coverability and volatility. Compared to the MST or NST powder mixed with 100% A, the same powder mixed with 100% W provided good coverability of the TiO_2 coating. This is because the absolute viscosity of water is higher than that of acetone. Figure 5 shows the influence of water or acetone on the air-drying time of the TiO_2 coating. The results show that the MST or NST powder mixed with 100% W produced poor volatility of the TiO_2 coating compared to the same powder mixed with 100% A. This is because the vapor pressure of water is much lower than that of acetone. Furthermore, these results show NST powder mixed with 100% W or 100% A provided good coating coverability, but poor coating volatility compared to the MST powder mixed with the same solvent, as nanoscale particles have a strong tendency to agglomerate.

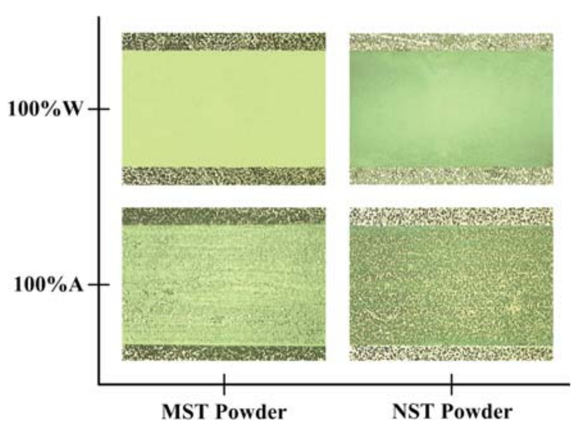

Figure 4. Appearance of TiO_2 coating obtained with various solvents.

The experimental results show that a single solvent cannot provide perfect coatability of the TiO_2 coating. Therefore, using a mixed solvent consisting of water and acetone that result in better coverability and volatility of the TiO_2 coating is advantageous. Note that an acetone is a volatile substance and that it mixes well with water. A mixed solvent of W/A was used in this trial. The designated mixing ratios of W/A were 20:80, 40:60, 60:40, and 80:20. Figure 6 shows the appearance of the TiO_2 coating obtained with the various mixed solvents.

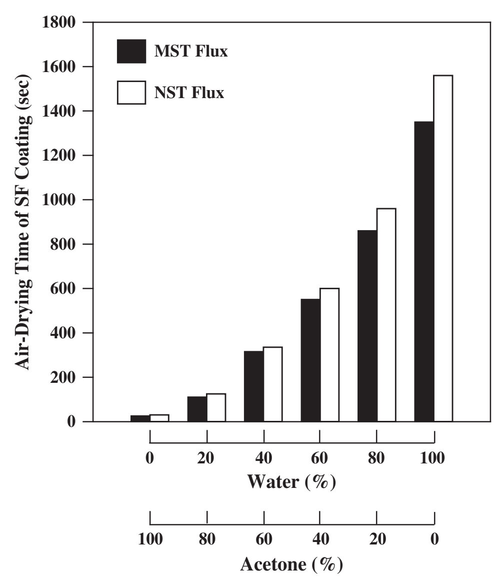

Figure 5. Influence of water or acetone on air-drying time of TiO_2 coating.

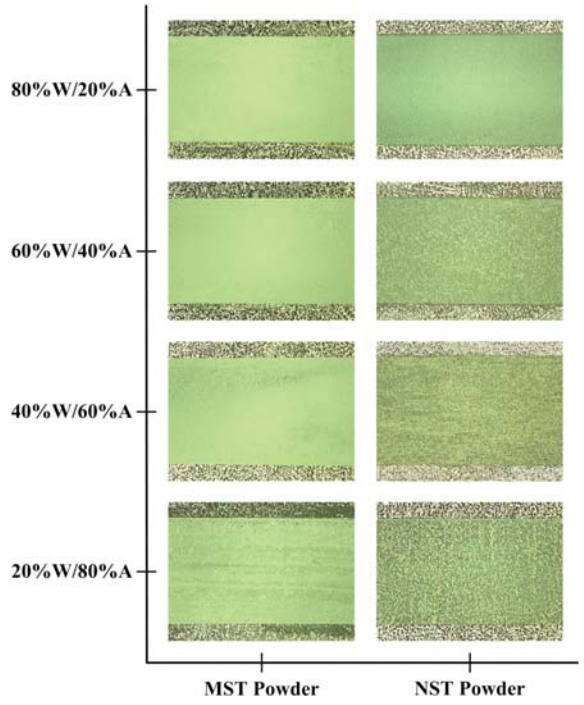

Figure 6. Appearance of TiO_2 coating obtained with various mixed solvents.

The results show that the MST powder mixed with the 60% W/40% A or 80% W/20% A provided better coverability of the TiO_2 coating, and that the NST powder mixed with the 80% W/20% A also provided better coverability of the TiO_2 coating. This study thus concluded that 80% W/20% A is an excellent solvent for mixing with both the MST and NST powders. Compared to the use of the 100% W, the advantage of using the 80% W/20% A is the potential to reduce the air-drying time of the TiO_2 coating. Another advantage of using the 80% W/20% A is the potential to produce a high-quality TiO_2 coating compared to using the 100% A.

3.3. Effect of TiO_2 Density on Depth of TIG-SF Weld

Various SF densities have different effects on the flow of liquid metal and transfer of arc heat energy in a MP, as well as on the depth of the TIG-SF welds. In this trial, 250 mg of MST or NST powder was mixed with 0.45 ml or 2.95 ml of the 80% W/20% A, respectively, to create a paste-like SF. The coated SF had a length and width of 160 mm and 12 mm, respectively. An autogenous, single-pass TIG welding procedure was used to make a bead-on-plate weld at various currents. The SF density (ρ_{SF}) is defined by the amount of the SF coating per unit area, given by the following formula:

$$\rho_{SF} = \frac{M_{w/} - M_{w/o}}{A}$$

where $M_{w/}$ is the mass of the specimen made with SF, $D_{w/o}$ is the mass of the specimen made without SF, and A is area of the SF coating.

Figure 7 shows the shape and size of UNS S17400 stainless steel TIG welds made with a TiO_2 density of 0 mg/cm^2 at various welding currents. The depth of the weld was 2.09 mm, 2.53 mm, and 2.88 mm at a welding current of 150 A, 200 A, and 250 A, respectively. In the TIG welding without TiO_2 of UNS S17400 stainless steel plate having 8 mm thickness, the depth was below 3 mm. Similarly, the width of the weld was 7.81 mm, 10.29 mm, and 12.59 mm at a welding current of 150 A, 200 A, and 250 A, respectively. When the welding current increased from 150 to 250 A, the depth of the TIG weld made without SF increased from 2.09 to 2.88 mm (an increase of 37.8%), as did its width from 7.81 to 12.59 mm (an increase of 61.2%). It was evident that a slight increase in the depth of the TIG weld made without SF occurred when the current increased, but its width became excessively wide. It is well known that the electromagnetic force (F_E), (aerodynamic) drag force (F_D), and thermocapillary force (F_T) drive the flow of liquid metal during the autogenous arc welding of steels. Over-increasing the current in the TIG welding without TiO_2 results in an expanded arc column and pulls the liquid metal radially outward due to a higher outward F_D. An expanded arc column also produces a lower downward F_E at the central region of the MP because of the lower density of the electric current. With a high welding current, the driving forces for liquid metal flow in a MP exhibit a low downward F_E, high outward F_D, and strong radial outward F_T, resulting in a shallow, wide shape of the weld.

Figures 8 and 9 show the relationship between the MST and NST flux densities and the TIG-SF weld depth at various welding currents, respectively. The TiO_2 density significantly influenced depth of the TIG-SF weld. At the same welding current, the depth of the TIG-SF weld initially increases with the MST or NST flux density and reaches a peak value, then remains approximately constant and subsequently decreases. The reason for this is that more arc heat energy will be consumed in breaking through the thick layer of TiO_2 coating. The barrier layer on the MP surface not only obstructs the transfer of the arc heat energy from the arc column to the base metal, but also reduces the fluidity of the liquid metal flow in a MP. When the arc heat energy is not high enough to penetrate the barrier layer, the depth of the TIG-SF weld will decrease consequently. To prevent the premature collapse failure of the coating layer of the TiO_2, the maximum amount of the coating layer of MST or NST flux was limited to approximately 10 mg/cm^2 and 5 mg/cm^2, respectively.

The results also indicate that the peak value of the TIG-SF weld depth depends on both the SF density and the welding current for the TiO_2 of the same particle size. At a welding current of 150 A, the peak depth

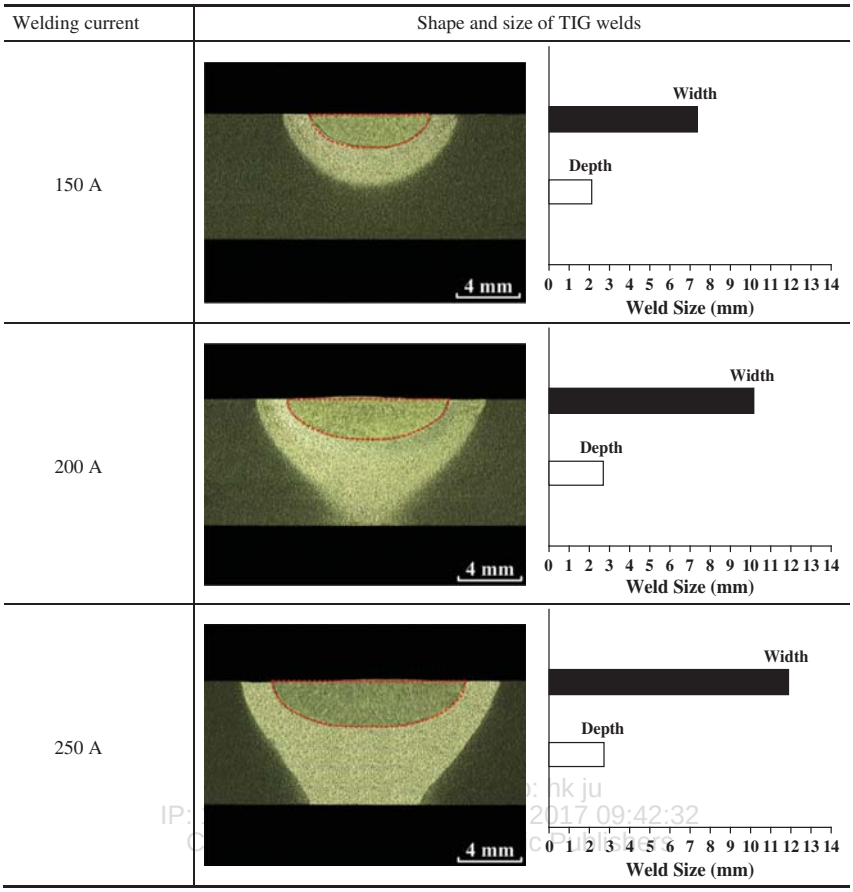

Figure 7. Shape and size of UNS S17400 stainless steel TIG welds made with TiO_2 density of 0 mg/cm^2 at various welding currents.

of 2.61 mm was obtained at a MST flux density of approximately 1.39 mg/cm^2, while the peak depth of 2.78 mm was obtained at a NST flux density of approximately 0.95 mg/cm^2. At a welding current of 200 A, the peak depth of 4.74 mm was obtained at a MST flux density of approximately 1.82 mg/cm^2, while the peak depth of 5.25 mm was obtained at a NST flux density of approximately 1.03 mg/cm^2. At a welding current of 250 A, the peak depth of 6.07 mm was obtained at a MST flux density of approximately 2.10 mg/cm^2, while the peak depth of 7.11 mm was obtained at a NST flux density of approximately 1.18 mg/cm^2. It can be seen that the MST or NST flux density does not significantly influence the depth of the TIG-SF weld under a welding current of 150 A for the UNS S17400 stainless steel plate of 8 mm thickness.

As seen in Figures 8 and 9, in the investigated current range of 150 to 250 A, the peak depth of the TIG-SF weld was obtained at a MST flux density between 1.39 mg/cm^2 and 2.10 mg/cm^2, or at a NST flux density between 0.95 mg/cm^2 and 1.18 mg/cm^2. The critical density of the SF for obtaining peak depth of the TIG-SF weld slightly increases with an increasing welding current for the TiO_2 ingredient of the same particle size. This study deduced that the higher arc heat energy requires a greater density of the SF in order to create an EIB at the MP surface. This is because higher arc heat energy leads to greater SF consumption. In the next section, we will describe the

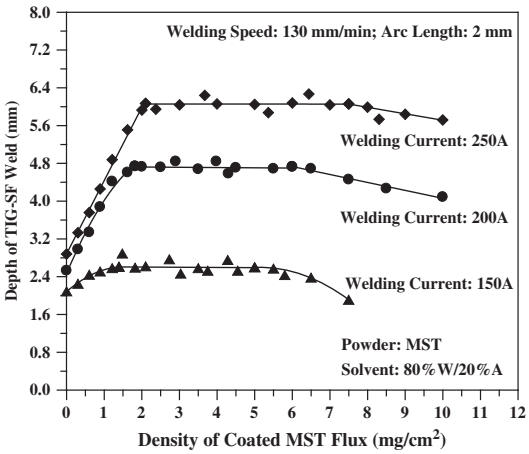

Figure 8. Relationship between density of coated MST flux and depth of TIG-SF weld at various welding currents.

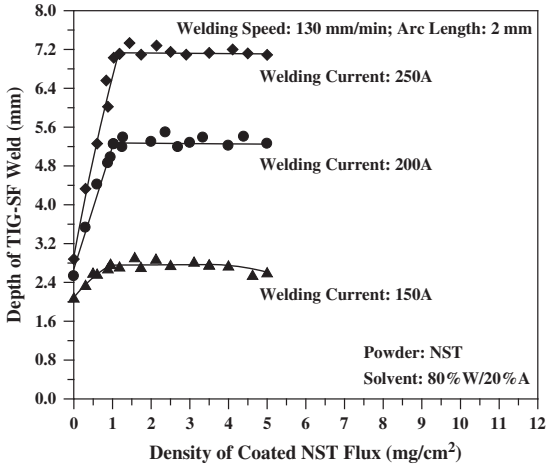

Figure 9. Relationship between density of coated NST flux and depth of TIG-SF weld at various welding currents.

features of an EIB. Comparing Figures 8 and 9 shows the critical density of the NST flux was lower than that of the MST flux at the same welding current. The results show the advantage of using nanoscale over microscale active oxides for the TIG-SF welding of stainless steel lies in the potential to reduce the amount of the SF coating.

3.4. Study on PC of TiO_2 Assisted TIG Welding

Figure 10 shows how the welding current influences the PC for the TIG-SF welding of UNS S17400 stainless steel. The PC is defined by the percentage change in the depth of the weld, given by the following formula:[6]

$$\mathrm{PC} = \frac{D_{w/} - D_{w/o}}{D_{w/o}} \times 100\%$$

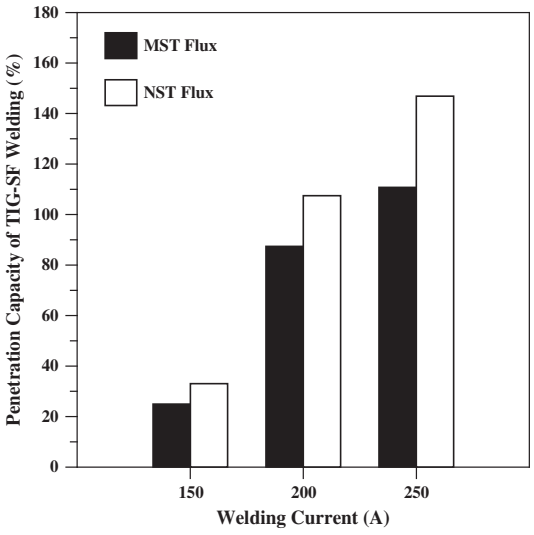

Figure 10. Influence of welding current on PC of TIG-SF welding of UNS S17400 stainless steel.

where $D_{w/}$ is the depth of the weld made with SF and $D_{w/o}$ is the depth of the weld made without SF.

There was a significant increase in the PC of the TIG-SF welding resulting from the use of a MST or NST ingredient, particularly at a high welding current. Although there is still no consensus regarding the mechanism responsible for increasing the PC of the TIG-SF welding, researchers have proposed three major theories: the reversed Marangoni convection caused by the temperature coefficient of surface tension, changed from a negative to a positive value.[16] The constricted arc column produced by the vaporized SF molecule, captured electrons in the outer regions of the electric arc.[17] The constricted arc column induced by the unmelted SF coating, reduced the flow of electric charge in the outer regions of the electric arc.[18] Figure 11 shows the view of an arc column of the TIG-SF welding. The arc column consists of two concentric zones: the arc plasma and the arc flame. The arc plasma is treated as an arc current channel because it carries most of electron in the arc column. By synthesizing the restricted arc current channel induced by an EIB and the reversed Marangoni convection, this study elucidated a physical mechanism for increasing PC in the TIG-SF welding of stainless steel.

Figure 12 shows a schematic diagram of an EIB. During the TIG-SF welding of steel, an EIB forms at the peripheral regions of the MP surface due to the difference in electrical resistance between the SF ingredient and the liquid metal.[7,18] The EIB has a high electrical resistance value and acts as a barrier against the flow of electric charge in the outer regions of the electric arc. The temperature of the electric arc at the central region of the MP surface will be sufficient to melt the coated SF so that the arc current can pass through the coating layer to the base metal. The arc current channel at the MP surface for TIG welding with SF tends to be restricted to a relatively narrow boundary zone by an EIB, as compared to TIG welding without SF. For a given current level, a restricted arc current channel

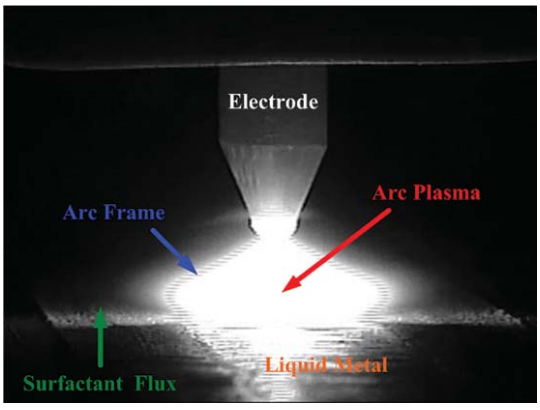

Figure 11. View of arc column of TIG-SF welding.

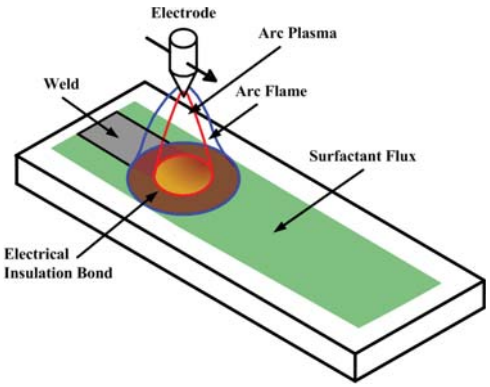

Figure 12. Schematic diagram of EIB during TIG-SF welding.

has a beneficial effect by increasing the downward F_E in a MP due to the increased current density at the central region of the MP, while also producing a lower outward F_D on the MP surface.

For the TIG-SF welding of steel, a low concentration of oxygen influences the direction of Marangoni convection by inverting the temperature coefficient of the surface tension in a MP. This is because dissolved oxygen present in a MP segregates preferentially to the surface of liquid iron.[19] Based on a previous study,[7] when the average OC in a low-carbon grade stainless steel TIG weld was more than approximately 60 ppm, the value of the temperature coefficient of the surface tension in a MP was positive. A change from a negative to a positive gradient of surface tension with temperature could reverse the direction of F_T from outward to inward circulation. Figure 13 shows the average OC in the UNS S17400 stainless steel TIG welds made with and without TiO_2. The ONH836 oxygen/nitrogen/hydrogen elemental analyzer was used to measure the OC in the UNS S17400 stainless steel weld. The readings were measured at three random locations of the weld, and then an average value was calculated for each case. The results show that the average OC in the TIG-SF weld increases with increasing welding current. When the welding current increased from 150 to 250 A, there were no significant changes in the average OC for the TIG weld made without SF, i.e., in the range of 40–45 ppm. At an investigated current of 200 A or 250 A, there exists sufficient OC (>60 ppm) in the UNS S17400 stainless steel TIG-SF weld. Consequently, the direction of circulation F_T would reverse, from radially outwards along the surface of the MP and up toward the pool top, to being radially inwards along the surface of the MP and down toward the pool bottom. At the investigated current of 150 A, the average OC in the UNS S17400 stainless steel TIG-SF weld was insufficient, resulting in a radial outward F_T in the MP. The results can be used to explain why there was no significant increase in the PC of the TIG-SF welding under a welding current of 150 A for the UNS S17400 stainless steel plate of 8 mm thickness. Figure 14 shows how the driving forces of liquid metal flow influence the joint penetration. An increase in the joint penetration would be obtained with a high downward F_E, low outward F_D, and radial inward F_T in a MP. The combination of a restricted arc current channel induced by an EIB and a reversed Marangoni convection leads to greater inward circulation and a downward flow of liquid metal towards the bottom of the MP. This in turn leads to an effective transfer of arc heat energy from the edge of the MP surface to its center, and subsequently down to the bottom of the MP. A higher PC can thus be expected in the MST or NST flux assisted TIG welding of UNS S17400 stainless steel.

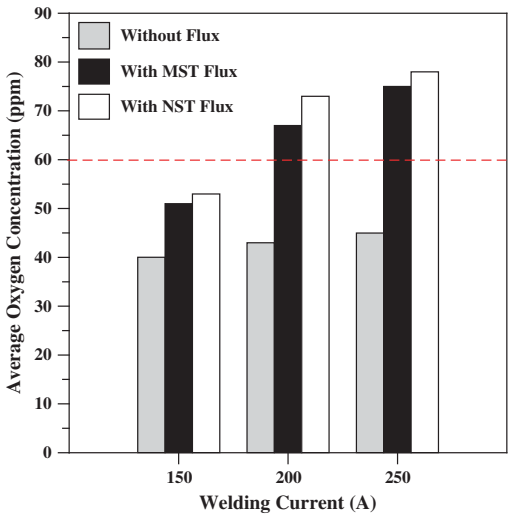

Figure 13. Average OC in UNS S17400 stainless steel TIG welds made with and without TiO_2.

Setting the current at 250 A results in the highest PC of the MST or NST flux assisted TIG welding of UNS S17400 stainless steel at 110.8% and 146.9%, respectively (Fig. 10). This result indicates the NST flux assisted TIG welding can better enhance the joint penetration compared to the MST flux. Two factors may cause the nanoscale particles to behave significantly differently from the microscale particles: surface and quantum confinement effects.[20] Compared to microscale particles, atoms situated at the surface of nanoscale particles have fewer direct neighbors, leading to a lower binding energy per atom.[21] A consequence of the reduced binding energy per oxygen atom is a lower Gibbs free energy of formation of oxides, i.e., the Gibbs free energy decreases with decreasing particle size.[22] It was evident that the NST ingredient exhibited a lower thermal stability than the MST ingredient. In addition, it is well known that the most prominent quantum confinement effect is the size dependence of the bandgap for nanoscale particles,[23] and the bandgap increases with decreasing particle size.[24] It was again evident that the

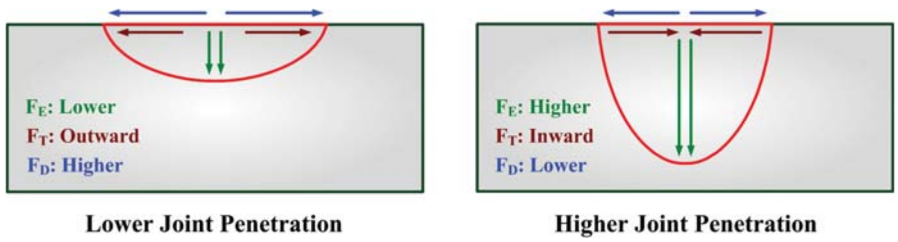

Figure 14. Influence of driving forces of liquid metal flow on joint penetration.

NST ingredient exhibited a higher electrical resistance than the MST ingredient.

This study concluded that the NST ingredient exhibited a higher electrical resistance, and thus more easily forming an EIB compared to the MST ingredient, resulting in a greater effect on restricting the arc current channel. This indicates that the flow of liquid metal exhibits a higher downward F_E and a lower outward F_D. The NST ingredient also exhibited a lower thermal stability, thus sufficient OC was more quickly obtained compared to the MST ingredient, resulting in a more pronounced reversed Marangoni convection. This indicates that the driving force for liquid metal flow in a MP exhibits a stronger radial inward F_T. Consequently, NST flux assisted TIG welding can further enhance the joint penetration compared to MST flux assisted TIG welding. The results indicate that the oxide used in the TIG-SF welding of stainless steels must have three key features: a high electrical resistance, low thermal stability, and small particle size.

4. CONCLUSIONS

MST and NST ingredients were used to investigate the PC of the TIG-SF welding of UNS S17400 stainless steel. The characteristics of the coated MST and NST ingredients were also evaluated and results compared. This study synthesized the restricted arc current channel induced by an EIB and the reversed Marangoni convection to elucidate a physical mechanism for increasing the PC of the TIG-SF welding of stainless steel. The findings obtained in the present study are summarized below:

1. Compared to the MST powder, the NST powder requires a significantly greater amount of solvent to create a paste-like SF. The preferred choice for the mixing ratio by weight of the MST powder to the solvent is 1:1.6, while that of the NST powder is 1:10.5.
2. In the preparation for obtaining TiO_2 coating, 80% W/20% A is the preferred solvent for mixing both the MST and NST powders, resulting in good coatability of the TiO_2 coating.
3. Under the same welding speed condition, the peak value of the TIG-SF weld depth depends on both the SF density and the welding current. Furthermore, the critical density of the coated SF depends on the heat energy of an electric arc for the TIG-SF welding.
4. To significantly increase the PC of the TIG-SF welding of stainless steels, a high-level of arc heat energy is desired. For a current set at 250 A, the highest PC of the MST or NST flux assisted TIG welding of UNS S17400 stainless steel is 110.8% and 146.9%, respectively.
5. During NST flux assisted TIG welding, an EIB is more easily formed and sufficient OC is also more quickly obtained. The use of NST ingredient can further enhance the PC of the TIG-SF welding of UNS S17400 stainless steel compared to the use of MST ingredient.
6. The potential benefits of TIG welding with nanoscale active oxides include a smaller amount of the coated SF and higher joint penetration. Based on the results obtained from the present work, a nanoscale active oxide is regarded as the best SF ingredient to use in the TIG-SF welding of UNS S17400 stainless steels.

Acknowledgments: The authors gratefully acknowledge financial support for this work from the Ministry of Science and Technology, Taiwan, R.O.C. under grant no. 103-2622-E-020-007-CC3.

References and Notes

1. K. Ozbaysal and O. T. Inal, *J. Mater. Sci.* 29, 1471 (**1994**).
2. K. H. Tseng and P. Y. Lin, *Materials* 7, 4755 (**2014**).
3. K. H. Tseng and K. L. Chen, *J. Nanosci. Nanotechnol.* 12, 6359 (**2012**).
4. K. H. Tseng, *Powder Technol.* 233, 72 (**2013**).
5. K. H. Tseng and N. S. Wang, *Powder Technol.* 251, 52 (**2014**).
6. K. H. Tseng and Y. J. Shiu, *Powder Technol.* 286, 31 (**2015**).
7. K. H. Tseng and P. Y. Chen, *Mater. Manuf. Process.* 31, 359 (**2016**).
8. M. Q. Johnson and C. M. Fountain, Penetration flux, US 6664508B1, December (**2003**).
9. K. H. Tseng, Welding flux for stainless steel, US 8394206B2, March (**2013**).
10. M. Q. Johnson and C. M. Fountain, Penetration flux, US 6707005B1, March (**2004**).
11. Y. Luo, Efficient active agent used for aluminum alloy alternating current TIG (tungsten inert gas) welding, CN 102886625B, June (**2015**).
12. Z. L. Liu, Y. F. Shen, J. Xu, and X. Q. Liu, Surfactant for magnesium alloy TIG welding and its prep process and usage, CN 100441365C, December (**2008**).
13. M. M. Najafpour, F. Rahimi, E. M. Aro, C. H. Lee, and S. I. Allakhverdiev, *J. R. Soc. Interface* 9, 2383 (**2012**).
14. T. Vossmeyer, L. Katsikas, M. Gienig, I. G. Popovic, K. Diesner, A. Chemseddine, A. Eychmiiller, and H. Weller, *J. Phys. Chem.* 98, 7665 (**1994**).

15. D. W. Wang, R. Chen, Q. Sun, and X. N. Li, *Materials* 8, 424 **(2015)**.
16. C. R. Heiple and J. R. Roper, *Weld. J.* 61, 97 **(1982)**.
17. W. Lucas and D. Howse, *Weld. Met. Fabr.* 64, 11 **(1996)**.
18. J. J. Lowke, M. Tanaka, and M. Ushio, *J. Phys. D: Appl. Phys.* 38, 3438 **(2005)**.
19. C. R. Heiple, J. R. Roper, R. T. Stagner, and R. J. Aden, *Weld. J.* 62, 72 **(1983)**.
20. A. L. Schoenhalz and G. M. Dalpian, *Phys. Chem. Chem. Phys.* 15, 15863 **(2013)**.
21. E. Roduner, *Chem. Soc. Rev.* 35, 583 **(2006)**.
22. S. Y. Xiong, W. H. Qi, B. Y. Huang, and M. P. Wang, *Chemphyschem.* 12, 1317 **(2011)**.
23. A. M. Smith and S. Nie, *Acc. Chem. Res.* 43, 190 **(2010)**.
24. G. Guisbiers, O. Van Overschelde, and M. Wautelet, *Appl. Phys. Lett.* 92, 103121-1 **(2008)**.

Received: 17 February 2016. Accepted: 23 March 2016.